Available online at www.sciencedirect.com
SCIENCE DIRECT®
International Journal of Rock Mechanics & Mining Sciences 43 (2006) 473–482
International Journal of Rock Mechanics and Mining Sciences
www.elsevier.com/locate/ijrmms

Precursors for rock fracturing and failure—Part I: IRR image abnormalities

Lixin Wu[a,b,c,*,1], Shanjun Liu[b], Yuhua Wu[b], Chuanyin Wang[a]

[a]*Institute of Rock and Soil Mechanics of The Chinese Academy of Science, P.R. China*
[b]*Institute of RS/GPS/GIS and Subsidence Engineering of China University of Mining and Technology, P.R. China*
[c]*Center for RS/GPS/GIS & Digital Mine Research, Northeastern University, Heping District, Shenyang, Liaoning Province 110004, P.R. China*

Accepted 7 September 2005
Available online 24 October 2005

Abstract

There are many precursors, including the abnormality of infrared radiation (IRR), for rock fracturing and failure. As the comprehensive effect of rock thermoelasticity and rock friction, the study of the IRR abnormality of loaded rock, as one of the important issues of remote sensing rock mechanics (RSRM), is facilitated by the fast development of IR remote sensing imaging technology. In view of energy input and consumption by the loading system, comprised of loader, rock and air, the mechanism of surface IRR from loaded rock is studied. The concepts that surface IRR is the comprehensive effect of a series of physical–mechanical processes inside loaded rock and that the thermoelastic effect and the frictional–thermal effect are two of the main mechanisms are presented here. Based on retrospective investigation of the fundamental experiments on RSRM during the past decade, it is concluded that there are two kinds of IRR abnormality as precursors of rock fracturing and failure: IRR image abnormality and IRR temperature curve abnormality. The spatial–temporal evolution of abnormal surface IRR images of loaded rock in a condition of uniaxial stress, compressive shear, biaxial stress, frictional slide and impact is systematically analyzed. The fact that large IRR can occur in the fracturing center of compressively loaded and shearing fractured strong and brittle rock is also revealed. Finally, the relation between rock stress and IRR temperature are studied based on thermomechanical coupling theory for solid materials. It is concluded that IRR image abnormalities are important precursors for rock fracturing and meaningful for the forecast of rockbursts and tectonic earthquakes.

Keywords: Remote sensing rock mechanics; Infrared radiation image; Abnormality; Thermomechanical coupling; Rock fracturing and failure; Precursor

1. Introduction

Rock fracturing is a natural phenomenon in geosciences and in rock engineering and includes tectonic earthquakes, rockbursts, rock slopes, rock pillar failure and coal pillar failure. The mechanism and the precursors of rock fracturing and associated 'catastrophe' are two important issues in rock mechanics, seismology and mining science. Many kinds of radiation signal, including acoustic emission [1,2], electromagnetic radiation [3], RF emission [4] and light radiation [3,5], emitted from fracturing rock, are able to provide important and useful information for interpreting and for predicting the behavior of rock fracturing, as well as the possibility of more severe rock catastrophe.

Luong [6] firstly studied the infrared radiation (IRR) of concrete in the process of loading and fracturing with thermal imaging technology. Based on real time and non-destructive detection with a thermal imager, Luong [7–9] studied the production and development of micro-fissures in the process of rock and concrete loading, fatiguing, fracturing and damaging. Geng et al. [10,11] showed the existence of IRR abnormality before rock fracturing in experiments for investigating the mechanism of satellite IRR abnormality before tectonic earthquakes [12,13]. Wu and Wang [14] found from thermal IRR imaging experiments on uniaxially loaded coal and sandstone specimens

*Corresponding author. Center for RS/GPS/GIS & Digital Mine Research, Northeastern University, Heping District, Shenyang, Liaoning Province 110004, P.R. China. Tel.: +24 83676786, +10 62331012; fax: +10 62331012.
E-mail addresses: wlx@cumtb.edu.cn, awulixin@263.net (L. Wu).
[1]Changjiang Professor of Ministry of Education of P.R. China.

1365-1609/$ - see front matter © 2005 Elsevier Ltd. All rights reserved.
doi:10.1016/j.ijrmms.2005.09.002

that there are three kinds of abnormal features for IRR thermal image and IRR temperature as precursors of rock failure, and that a stress level of around $0.79\sigma_c$ could be taken as a 'precaution index' for the stability monitoring of coal and rock. Later, a large amount of IRR imaging experiments on rock fracturing was conducted in China [15–23]. A new inter-disciplinary topic, remote sensing rock mechanics (RSRM), which takes remote sensing, rock mechanics, rock physics and informatics as its scientific and technical disciplines and serves for geosciences, rock mechanics and rock engineering, originated in the 1990s [10,15].

Many IRR abnormal images and IRR abnormal temperature data were recorded, and their meanings for rock fracturing and failure were studied. Aiming to compare the IRR abnormalities as precursors for different rock fracturing and failure, the abnormal IRR images from IRR detection experiments on rock samples in conditions of uniaxial loading, biaxial loading, compressive-shear loading and Hopkinson impacting bar are analyzed. Based on the physical mechanism discussions on IRR from loaded rock, this paper emphasizes systematical analysis of the spatial–temporal evolution of IRR images and the large amount of IRR which occurs in the fracturing center of rock samples. For theoretical interpretation, the relation between rock stress and IRR temperature is studied based on thermomechanical coupling theory for solid materials.

2. Mechanism of surface IRR from loaded rock

As a relatively independent closed system, comprised of loader head, rock sample and environmental air, as shown in Fig. 1, rock deformation, rock fracturing and rock failure are a complex process of energy input and consumption. Without consideration of the possible chemical reactions and related energy changes inside loaded rock, the energy input to loaded rock includes two parts: the mechanical work of the loading actuator and the heat input through positive thermal exchange from the actuator head and environmental air. The energy consumption by the loaded rock is much more complex in that it includes the energy accumulation in the rock and energy dissipation from the rock.

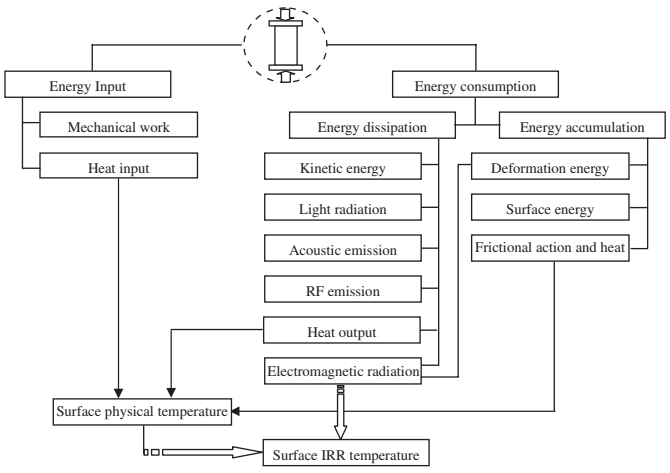

Fig. 1. IRR mechanism related to energy accumulation and consumption by loaded rock.

The energy accumulation in the loaded rock includes the positive elastic–plastic deformation energy of rock (the positive change of oscillation and rotation energy of mineral molecules), the surface energy of newly produced fractures or fissures, and the frictional actions between mineral molecules, grains, joints, fissures and fractures inside the rock as well as the produced frictional heat. The energy dissipation from the loaded rock includes the negative thermal exchange with the loader head and/or environmental air (i.e., heat output), the kinetic energy of flying fragments of fractured rock, light radiation, acoustic emission, RF emission and electromagnetic radiation including IRR and microwave radiation.

Since thermal exchange (heat input and output) and frictional action cause the loaded rock to change its heat state, the rock surface physical temperature, without consideration of the complex heat transfer process inside the rock, could be a direct index reflecting the heat state of the loaded rock. The Stefan–Boltzmann formula states that the IRR strength (radiation flux density) of any material, at temperatures above absolute zero, is biquadratic to its surface physical temperature. Crystal physics states that the energy jump of molecules oscillation and/or rotation due to the change of molecules distance, resulting from deformation, is an important mechanism of electromagnetic radiation. Hence, the rock surface IRR is a comprehensive effect of rock deformation and the physical thermal state of the rock surface. The rock surface IRR temperature could be an index reflecting the rock surface physical temperature and rock surface deformation field, which indicates the complex physical–mechanical process inside loaded rock.

In spite of thermal exchange and plastic deformation, the thermoelastic effect and the frictional–thermal effect [24] are two of the main physical mechanics of IRR production from loaded brittle rock. In the stage of elastic deformation, the thermoelastic effect is the main cause, while in the stage of plastic deformation or fracturing, the frictional–thermal effect plays a great role. At the moment of rock fracturing or failure, the friction-heat effect becomes more significant. The friction-heat effect depends on two factors: frictional force (decided by normal stress and frictional coefficient) and frictional speed. The larger the frictional force and the quicker the frictional speed, the stronger the frictional heat effect.

3. Spatial–temporal evolution of IRR image abnormality

3.1. Uniaxially loaded rock

Many rock samples of coal, ironstone, sandstone, marble, limestone, granite, granodiorite, gabbro and gneiss

were uniaxially loaded and IRR imaging detected. The sample size was standard, diameter 50 mm and length 100 mm. It was discovered that the surface IRR image of the loaded rock has different features for different fracturing patterns. Three fracturing patterns, "X"-shaped, "／／"-shaped and "|"-shaped, occurred in our experiments. The "X"-shaped and "／／"-shaped positive IRR image abnormal strip-group foretells the coming of an "X"-shaped shearing fracture and the coming of a "／／"-shaped shearing fracture, respectively, while the "|"-shaped negative IRR image abnormal strip foretells the coming of tensile fracture. The typical surface IRR image abnormalities as precursors of rock fracturing are shown in Figs. 2–4.

The "X"-shaped positive IRR image abnormal strip-group occurs along the "X"-shaped shearing zone before peak stress and gets distinguished after peak stress, as in Fig. 2. The rock sample will finally fracture along the "X"-shaped shearing zone. It is discovered that the fracturing is not symmetrical upper-and-lower, i.e., the upper part of the loaded rock fractures more than the lower part. The temporal–spatial evolution of the IRR image abnormal strip-group, as in Fig. 2, also reflects the asymmetrical fracturing. The upper part of the strip group is clear and bright with higher radiation temperature, while the lower part of the strip group is fuzzy and dark.

The "／／"-shaped positive IRR image abnormal strip-group occurs along the "／／"-shaped shearing zone at the upper part of the rock sample before the peak stress and increases after the peak stress, as in Fig. 3. The temporal–spatial evolution of the positive IRR image abnormality also reflects the asymmetrical fracturing. The upper part of the strip group is clear and strong with higher radiation temperature, while the lower part of the strip group is fuzzy and dark, except for the final fracturing near the bottom of the sample. Besides, there is a strong IRR spot at the fracturing center indicating the intensive accumulation of mechanical energy and the intensive generation of friction heat at the central location.

The "|"-shaped negative IRR image abnormal strip occurs along the tensile fracturing zone of the rock sample before the peak stress and will get clear gradually at the peak stress and after fracturing, as the approximately vertical dark strip in Fig. 4. The same phenomenon for a sandstone sample with a calcite vein was reported [15].

3.2. Uniaxially loaded rock with a central hole

More than ten central-holed samples, modeling a rock tunnel, made from marble and granite, were IRR imaging detected in the condition of uniaxial load. The rock samples had two kinds of shapes: one shape was a standard cylinder with diameter and length, respectively, 50 and 100 mm; the other shape was a regular block with thickness, width and length, respectively, 70, 35 and 100 mm. It is discovered that there are strong positive

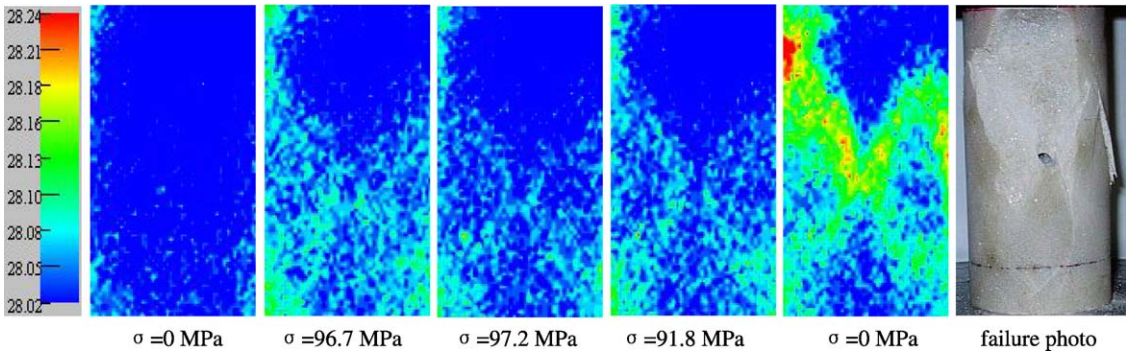

Fig. 2. Infrared radiation precursor of "X"-shaped shearing fracture of uniaxially loaded marble.

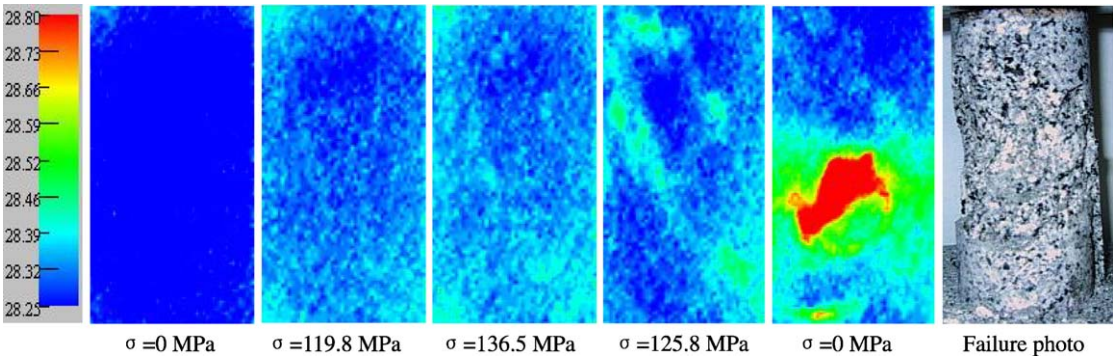

Fig. 3. Infrared radiation precursor of "／／"-shaped shearing fracture of uniaxially loaded granite.

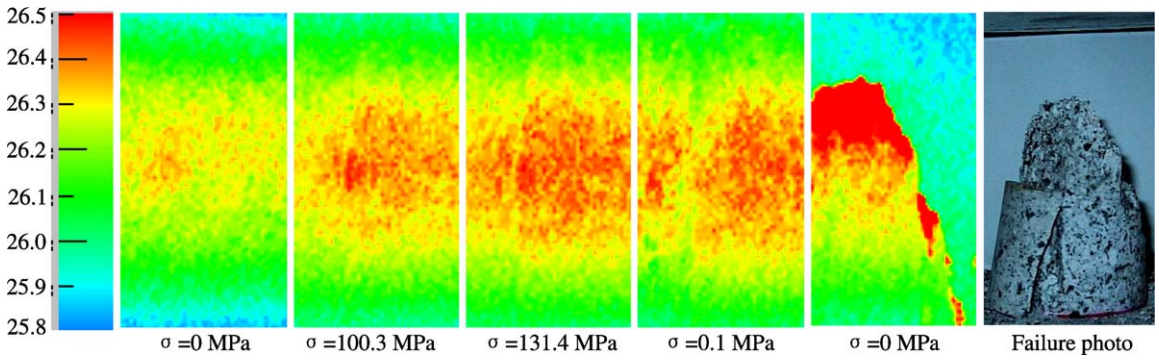

Fig. 4. Infrared radiation precursor of "|"-shaped tensile fracture of uniaxially loaded granite.

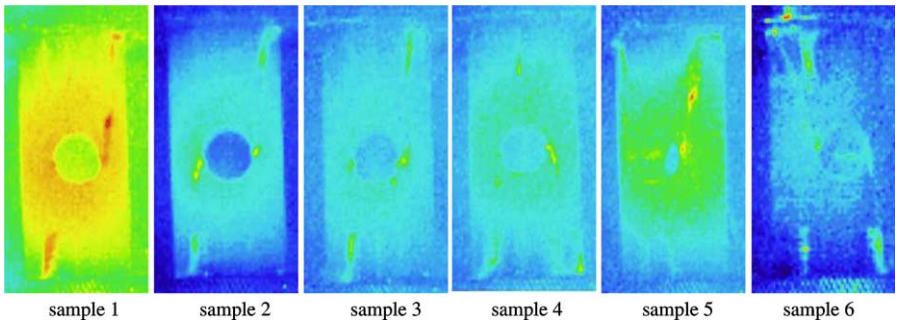

Fig. 5. Positive IRR abnormality for different fracture patterns of uniaxially loaded central-holed marble.

IRR image abnormities before the fracturing of rock samples, and the location of the IRR image abnormities is exactly the future fracturing location.

As shown in Fig. 5, the positive IRR image abnormalities reflect two fracturing patterns of central-holed rock samples, i.e., diagonal fracturing (samples 1, 2, 3, 5 and 6) and fork fracturing (sample 4). The positive IRR image abnormality along the fracturing plane as spots or strips occurs not only on the outside surface of the rock sample but also on the inside surface of the hole (samples 5 and 6). The temperature increment of the IRR image abnormality is 1–3 K and 4–8 K, respectively, for marble and granite. It is concluded that IRR imaging is a possible and potential remote sensing detection method for rock fracturing and structure stability prediction in rock tunnel excavations.

3.3. Compressively sheared rock

More than 20 samples, size $7 \times 7 \times 7\,\mathrm{cm}^3$, made from sandstone, marble, limestone, granite and gneiss, were compressively sheared and IRR imaging detected. Three pairs of steel platens with shearing angles, respectively, being 45°, 60°and 70° were applied. A Changjiang-200 presser was applied for manual-controlled loading at a rate 2–5 kN/s, and the IRR image recording rate applied was 1 frame/s. It was discovered that the IRR temperature of the rock surface changes with loading, and strip-shaped positive IRR image abnormality will develop along the central shearing plane before fracturing. With loading, the positive abnormal strip becomes more and more evident and migrates from the upper end to the lower end gradually, which indicates that the compressive-shearing fracturing is developing gradually from the upper end to the lower end along the central shear plane. Fig. 6 shows the typical IRR image series of a compressively sheared limestone sample.

As a special geological dynamic-mechanical phenomenon occurring with the formation of a larger fault, penniform fractures are a group of secondary fractures produced with the formation of the primary fracture [25]. It happened to occur in our experiments that there are penniform fractures accompanying primary fracture in the compressive-loaded rock samples. As in Fig. 7, the positive IRR image abnormal strips occurring aside the primary IRR strip, along the central shearing plane, show that the penniform fractures are produced with the formation of the primary fracture.

3.4. Biaxially loaded rock

To study the mechanism of satellite remote sensing IRR image abnormalities occurring with some middle-to-strong tectonic earthquakes, IRR imaging detection on the rupturing of modeled discontinuous jointed faults, en echelon faults and collinearly disconnected faults was experimentally studied in the process of biaxial loading [18], as in Figs. 8 and 9.

It is revealed from the experiments that the IRR of a loaded rock surface is correlated with the loading stress, which can be divided into five stages as loading

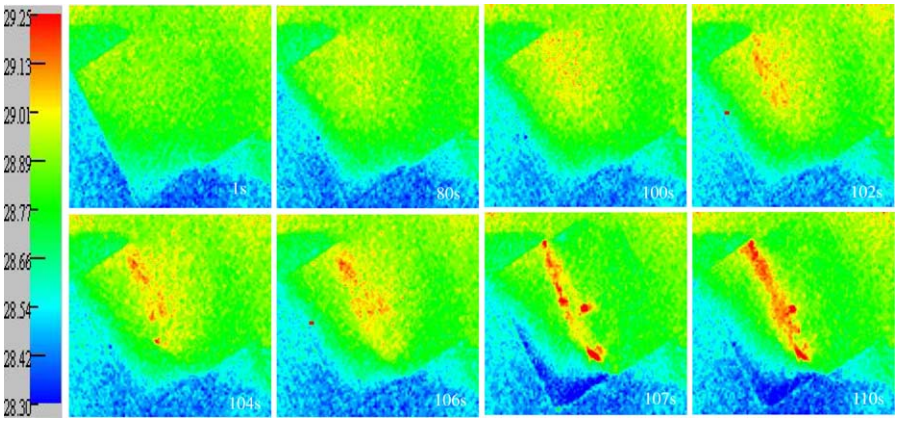

Fig. 6. IRR precursor of fracturing of compressively sheared limestone.

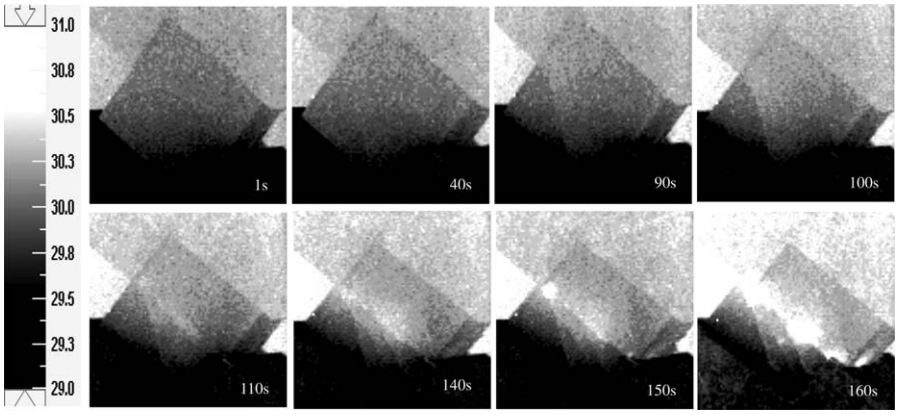

Fig. 7. IRR precursor of penniform fracturing of compressively sheared marble.

commences, linear elasticity, stress locking, stress unlocking and fracturing [18]. During the stage of stress unlocking, the positive IRR image abnormal strip will occur at the discontinuous locations of en echelon faults and discontinuous faults, as in Figs. 8 and 9. The positive IRR image abnormal strip of the discontinuous faults has the spatial–temporal evolution features as: firstly, the strip is enhanced; then, becomes weaker (or 'silence'); and finally, enhances again. The re-enhancing of the IRR image abnormal strip after the weakening stage is a meaningful precursor foretelling the location of primary fracturing or the hypocenter of the coming shock or earthquake.

3.5. *Bi-sheared friction sliding rock blocks*

The frictional sliding or the viscosity sliding of bi-sheared rock blocks is another important mechanism of tectonic earthquake and rock structure failure. Ten groups of composed rock blocks made from gabbro, granodiorite, limestone and marble were IRR image-monitored in the process of bi-sheared frictional sliding. Each group, as in Figs. 10 and 11, comprised of three rock samples whose size was $50 \times 50 \times 100$, $50 \times 70 \times 150$ and $50 \times 50 \times 100\,\mathrm{mm}^3$ from left to right, and the contacting area was a constant, $50 \times 100\,\mathrm{mm}^2$. Four kinds of contact conditions, symmetrical (yes for rock property and for its smooth friction surface), uncertain symmetrical (yes for rock property but not for its coarse friction surface), unstable asymmetrical (yes for rock property material but not for its staged friction surface) and stable asymmetrical (not for rock property but yes for its smooth friction surface), were designed and tested [19].

It is revealed from the experiments that the temporal–spatial evolution of the surface IRR temperature field of the rock samples is not only correlated with rock stress but also correlated with the features of the frictional surface as well as the rock properties at both sides. The IRR is stronger at the location of stress concentration and strong friction zone than that at the location of stress relaxation and weak friction zone. For the condition that the friction surface be symmetrical, the IRR image is double butterfly wing-shaped, as in Fig. 10; while in the condition that the friction surface be uncertain symmetrical, unstable asymmetrical and stable asymmetrical, the temporal–spatial evolution of IRR abnormality is uncertain or unstable for the asymmetrical and disequilibrium variation of the IRR image with sliding, as in Fig. 11 for the uncertain symmetrical. The positive IRR image abnormal spots may

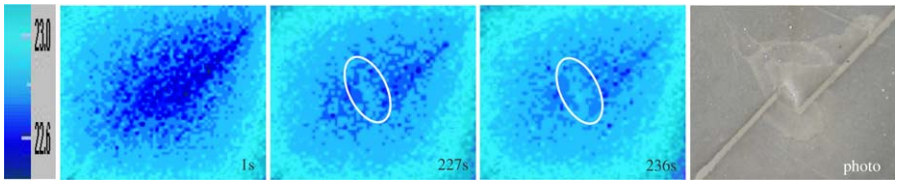

Fig. 8. The local IRR positive abnormality foretell the fracturing of en echelon faults (marble).

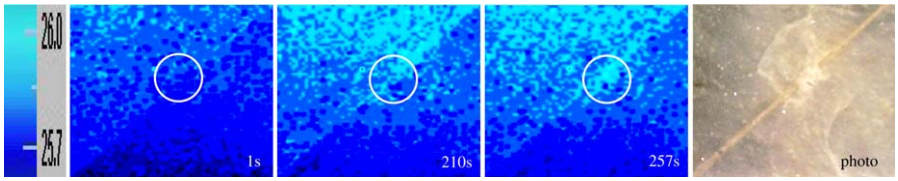

Fig. 9. The local IRR positive abnormality foretell the fracturing of collinear disconnected faults (marble).

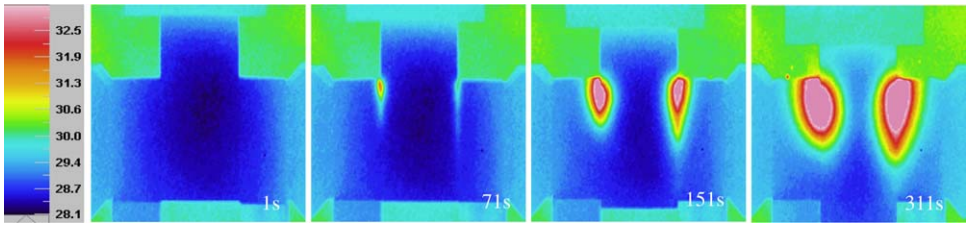

Fig. 10. IRR precursor of the stick–slip of symmetrical rock blocks.

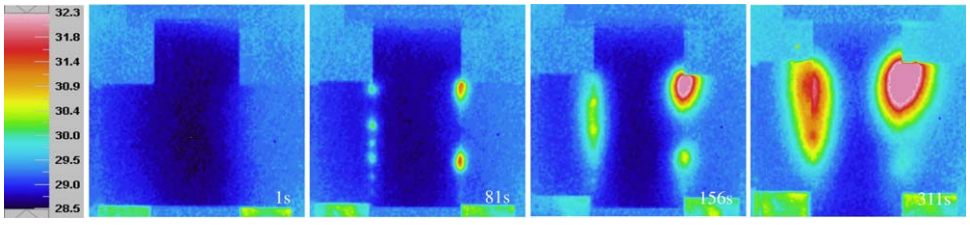

Fig. 11. IRR precursor of the stick–slip of asymmetrical rock blocks.

be bead-shaped, needle-shaped, suspended needle-shaped, strip-shaped, single butterfly wing-shaped or its evolution in order [19]. It foretells the temporal–spatial evolution of stress concentration, energy conversion and potential viscosity sliding or fracturing along the sliding surface.

3.6. Impacted rock

A large amount of IRR imaging detections on the transient process of marble and granite being normally impacted was conducted [16,21]. Free fall impaction by steel ball and Hopkinson impaction bar by steel projectile were applied. The diameters of the steel balls are different from $\Phi = 7$ to 25.4 mm, and the falling height varied from 0.3 to 2 m [16]. The size of the steel projectile is diameter $\Phi = 13$ mm and length $L = 50$ mm, and its impacting velocity powered by a Hopkinson bar varied from 7.5 to 25 m/s [21]. It was revealed from the experiments that the positive IRR image abnormality on the rock target is tightly correlated with the ball's falling height or the projectile's speed and impacting angle. There exists a critical velocity at normal impaction for the target's IRR temperature field being central symmetrical within the velocity. For the marble target the critical velocity is 15 m/s.

Within the critical velocity of Hopkinson impact, the positive IRR abnormal spot of the normally impacted rock target is approximately circular. The size, brightness and IRR strength of the spot increases with the bullet's velocity, as in Fig. 12. The effect of the impacting angle on the IRR image is complex, as in Fig. 13 (here the angle 0° indicates normal impact). The brightness or the IRR strength of the spot increases with the impacting angle and reaches its peak at angle 45°; then it decreases with the angle, until the angle gets nearly parallel to the rock surface. It indicates that the energy conversion from the bullet's mechanical energy to frictional heat and IRR energy depends on the impact angle, i.e. the normal impact

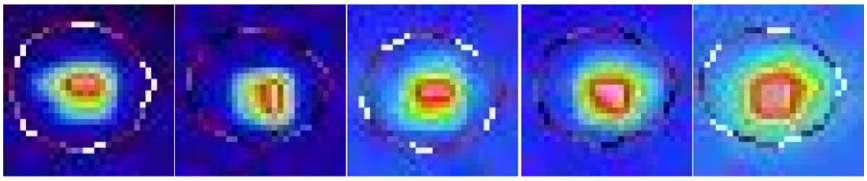

Fig. 12. Positive IRR spots of normally impacted marble within the critical velocity.

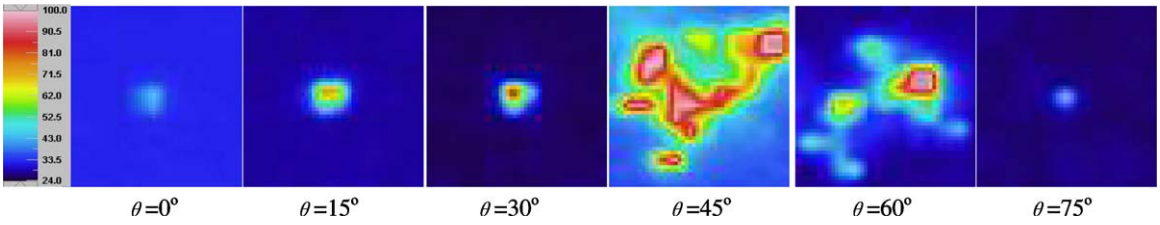

Fig. 13. Positive IRR spots of impacted marble at different angles within the critical velocity.

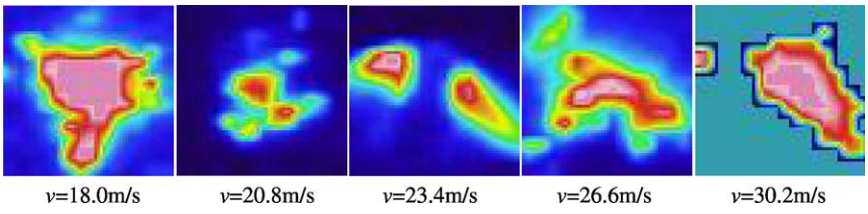

Fig. 14. Positive IRR spots of normally impacted marble beyond the critical velocity.

has the weakest effect on the rock surface IRR, while the 45° impact has the strongest effect on the rock surface IRR.

Beyond the critical velocity, the positive IRR image abnormality of the normally impacted rock target zone is random and complex because of the fracturing of the rock target, as in Fig. 14. Hence, the asymmetrical and complex-shaped positive IRR image of the rock target is informative in that it shows that the rock target has been damaged by the bullet, i.e. the impacting velocity is beyond the critical velocity of the current rock sample.

4. Large IRR at the fracturing center

As the recording rate of the IRR imager applied was 60 frame/s, the transient IRR temperature at the fracturing center was recorded. In the condition of uniaxial loading, the fracturing center of brittle rock is at the inside center of the "X"-shaped fracturing, while in the condition of compressive shearing at a high angle, 60° and 70°, the fracturing center is the center of the fractured shearing region exposed to the IRR imager immediately after the fracturing.

It was discovered that the transient IRR temperature at the fracturing center of uniaxially loaded rock is much higher than that on the rock surface, as in Fig. 15, and it is correlated with rock strength and rock deformation. The higher the rock strength and/or the more the deformation, the larger the central temperature. For some hard rock samples made from gabbro and gneiss, the transient IRR temperature at the fracturing center of compressively sheared rock is higher than 155 K, which is the upper limitation of the second temperature range (72–155 K) of the IRR imager applied. If the third temperature range (155–300 K) were applied, much higher transient fracturing temperature should have been detected.

In the condition of high-angle compressive shearing, the ruptured upper block of some rock samples was pushed apart from the steel platen immediately after the abrupt rupturing, usually 1–2 s after the rupturing. Hence, the inside shearing region was exposed to the IRR imager immediately and the transient IRR temperature field of it was recorded. It is discovered that the IRR temperature on the inside shearing region is not only much higher than that on the outside rock surface, but also inhomogeneously distributed, neither even nor centripetal, as in Fig. 16. This means that much more mechanical energy had been converted into IRR energy and frictional heat due to intensive energy accumulation, sufficient local deformation and abrupt frictional sliding at the shearing center. In other words, the large IRR temperature at the inside shearing center indicates the comprehensive effect of local concentrated energy conversion and frictional heat.

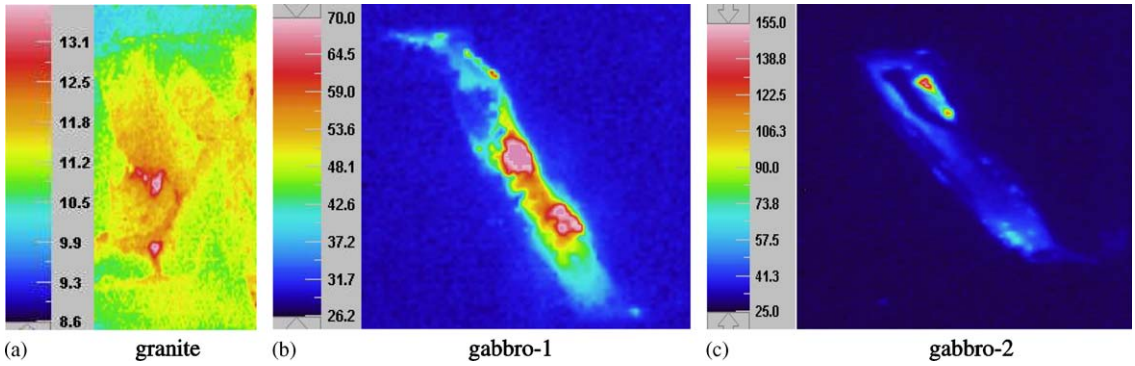

Fig. 15. Transient IRR imaging of the fracturing rock uniaxially loaded (a) and compressively sheared (b and c).

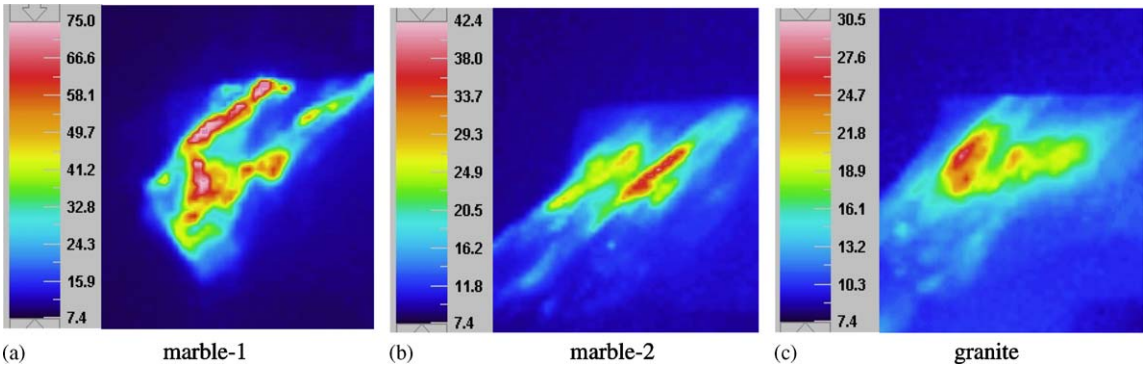

Fig. 16. Transient IRR isothermal field inside the fracturing surface of compressively sheared rock.

Hence, it could be deduced that, in the condition of large tectonic stress, larger deformation and/or abrupt frictional slide, tremendous rock temperatures, as high as hundreds or thousands of degrees Celsius inside an active or fracturing crust rock, are possible. The high temperature could cause partial melting of the rock, and provide a scientific explanation for the existence of pseudotachylyte in some larger faults [25–27] and for the failure-generated EQLs [4]. The EQLs generally refer to the mysterious earth fire and strong light along some new-generated fracturing fissures at the moment of larger tectonic earthquakes. Also, it could be deduced that the continuous shearing deformation or the abrupt fracturing of a highly loaded rock or coal body in a coal mine could cause local shear heating of temperature as high as hundreds of degree Celsius, which might cause ignition of local methane (the minimum ignition temperature is 595 °C) which would then develop into a catastrophic gas explosion.

5. Theoretical interpretation

5.1. Thermomechanical coupling in a solid

The heat production in a solid due to stress action is termed the thermomechanical coupling effect. According to the features of solid material and the different deformation stages of a loaded solid, thermomechanical coupling is classified as thermoelastic, thermoplastic and thermoviscous, respectively, for elastic deformation, plastic deformation and viscous deformation. Since the tested rock is hard, dry and brittle in our experiments, its plastic and viscous deformation could be ignored. Hence, thermoelastic effect and friction heat are the two chief mechanisms of surface IRR from loaded rock. Kelvin developed the thermoelastic theory in 1853 [24]. It was stated that the physical temperature change of a loaded component is correlated to its stress change as:

$$\Delta T/T = -K_0 \Delta\sigma. \tag{1}$$

Here, T is the absolute temperature of loaded component (K), ΔT is the change of temperature (K), K_0 is the thermoelastic factor (MPa^{-1}), and $\Delta\sigma$ is the change of the sum of the three principal stresses ($\Sigma\sigma_i$ ($i = 1, 2, 3$), MPa).

Based on thermoelastic theory, two technologies, thermoelastic stress analysis (TSA) and stress pattern analysis by thermal emission (SPATE) [28], were developed for the stress measurement of solid materials in the 1960s and 1970s. Nowadays, TSA and SPATE have been widely applied in experimental solid mechanics for homogeneous metal, macromolecular and composite materials.

As for an isotropic linear elastic solid, the surface physical temperature variation of a solid component is tightly correlated with the sum of two principal stresses

($\Sigma\sigma_i$, $(i = 1, 2)$):

$$\Delta T = -\frac{\alpha}{\rho C_p} T\,\Delta(\sigma_1 + \sigma_2). \quad (2)$$

Here, T is the surface absolute temperature of loaded solid (K), ΔT is the change of temperature (K), α is the factor of linear expansion (K^{-1}), ρ is the solid density ($kg\,m^{-3}$), C_p is the thermal capacity of solid at normal atmosphere ($J\,kg^{-1}\,K^{-1}$), and σ_1 and σ_2 are the two principal stresses of rock surface (MPa). The thermoelastic factor K is defined as $K = -\alpha/\rho C_p$.

For stress measurement with TSA and SPATE, the relation between the stress increment and the IRR signal based on Eq. (2) is [28]

$$\Delta(\sigma_1 + \sigma_2) = A_{\text{th}}\,\Delta S,$$
$$\Delta S = \Delta(\sigma_1 + \sigma_2){A_{\text{th}}}^{-1}. \quad (3)$$

Here, A_{th} is a comprehensive factor called the corrective factor, which is a function of solid surface emissivity, solid surface physical temperature, solid thermoelastic factor and three parameters related to the IRR detector, (units in $MPa\,U^{-1}$). ΔS is the increment of thermoelastic voltage signal detected (U).

However, for the complex composition of rock material and for its inhomogeneous features, the application of TSA and SPATE for rock was rarely reported. It was not until the end of the 1980s that IRR imaging technology was applied in rock mechanics. Nowadays, many IRR features from loaded and fracturing rock are being experimentally discovered and reported, and research on RSRM is developing from qualitative analysis to quantitative calculation [16,17,21,22]. The theoretical interpretation for IRR from loaded, deforming and fracturing rock has been a hot issue in RSRM.

5.2. Thermomechanical coupling in a rock

If the slight change in rock surface emissivity, rock thermoelastic factor and the IRR detector's parameters during rock loading could be ignored, and if the change of rock surface physical temperature cannot be ignored due to the thermal exchange and frictional heat as shown in Fig. 1, the relation between A_{th} and the dynamically changed rock surface physical temperature can be expressed as $A_{\text{th}} = \beta T^{-1}$. The detected IRR signal S is a direct representation of surface IRR temperature, i.e., $\Delta \text{IRR}T = \gamma\,\Delta S$. Hence, the following equation for IRR temperature and rock surface stress is deduced from Eq. (3) as

$$\Delta \text{IRR}T = \gamma\beta^{-1} T\,\Delta(\sigma_1 + \sigma_2). \quad (4)$$

Here, $\Delta \text{IRR}T$ is the detected IRR temperature (K), β is a constant correction factor related to rock surface emissivity, rock thermoelastic factor and three parameters of IRR detector (units in $MPa\,K\,U^{-1}$), and γ is a transfer factor between detected voltage signal and IRR temperature ($K\,U^{-1}$).

It means that, in Eq. (4) the IRR temperature increment of the rock surface is a direct reflection of the incremental sum of the two principal stresses on the rock surface. If no frictional heat is produced and the thermal exchange is stable, the IRR temperature of the rock surface is to rise with loading, and the spatial–temporal evolution of the surface IRR image will be stable. If there is no frictional heat produced but the thermal exchange is unstable, the surface IRR temperature will be unstable, and the spatial–temporal evolution of the surface IRR image will also be unstable. If there is frictional heat produced and conducted to the rock surface, both the thermal exchange and the surface IRR temperature of the rock surface will be unstable, and the spatial–temporal evolution of the surface IRR image will get complicated, as in Figs. 2–4, 7, 8, 11.

Especially in conditions of compressive shearing and friction slide, there is a large amount of frictional heat produced in the friction zone, which causes the rise of physical temperature in the friction zone. The physical temperature of the rock surface will also rise if the thermal conduction from the friction zone can reach the rock surface. Hence, the IRR image abnormality will be strong and sometimes large as a combined effect of rock stress and frictional heat, as in Figs. 5, 6, 9, 10, 14 and 15.

6. Conclusions

There are two important rock physics mechanisms thermomechanical coupling and frictional heat, for the change of thermal parameters in loaded rock. As a kind of indicator remote sensing electromagnetic signal and as linearly correlated with rock stress and physical temperature, IRR is potentially a meaningful index for the study of rock load, rock deformation, rock fracturing and rock 'catastrophe'. The IRR image abnormality referring to the spatial–temporal evolution of IRR from a loaded rock surface is an important precursor for rock fracturing and failure. Being an important issue in remote sensing rock mechanics, the potential application of IRR imaging in experimental rock mechanics, rock engineering, mining science and seismology includes remote sensing detection of rock stress and the forecast of more severe rock 'catastrophes'.

Acknowledgements

The research on RSRM has been continuously excited and encouraged by many scientists including academicians J.A. Hudson, M.G. Qian, D.R. Li, X.R. Ge, S.N. Zhou, Y.T. Chen, J. Ma, and Prof. N.G. Geng, C.Y. Cui, B.J. Fu, X.T. Feng and K.J. Wang. This research is supported by The Foreland Fundamental Research Funds (Ratified no. Q110307) of IRSM-CAS, The National Excellent Ph.D. Dissertation Funds (Ratified no. 200046), The National Natural Science Funds of China (Ratified no.10172090), and The Natural Science Funds of Beijing Municipal (Ratified no. 8001003).

References

[1] Hardy HR. Application of acoustic emission techniques to rock mechanics research. Am Soc Test Mater Spec Tech Publ 1972;505: 41–83.

[2] Yamada I, Masuda K, Murakami H. Electromagnetic and acoustic emission associated with rock fracture. Phys Earth Planet Interior 1989;57:157–68.

[3] Renata D. Electromagnetic phenomena associated with earthquakes. Geophys Surv 1977;3:157–74.

[4] Martelli G, Smith PN, Woodward AJ. Light, radiofrequency emission and ionization effects associated with rock fracture. Geophys J Int 1989;98:397–401.

[5] Brady BT, Rowell GA. Laboratory investigation for the electrodynamics of rock fracture. Nature 1986;321(29):488–92.

[6] Luong MP. Infrared observation of failure processes in plain concrete. Durability of building materials and component. DBMC, 4 November 1987, Singapore:Pergamon. p. 870–78.

[7] Luong MP. Infrared thermovision of damage processes in concrete and rock. Eng Fract Mech 1990;35(1-2-3):127–35.

[8] Luong MP. Infrared thermographic observations of rock failure. Comprehensive rock engineering principles, practice and projects, vol. 4, Oxford:Pergamon;1993. p. 715–30 [chapter 26].

[9] Luong MP, Eytard JC. Infrared thermovision of dissipation in concrete and concrete works. Génie Parasismique et Réponse Dynamique des Ouvrages 1999;AFPS II:471–8.

[10] Geng NG, Cui CY, Deng MD, et al. Remote sensing detection on rock fracturing experiment and the beginning of remote sensing rock mechanics. Acta Seismol Sin 1992;14(Suppl.):645–52.

[11] Geng NG, Yu P, Deng MD, et al. The simulated experimental studies on cause of thermal infrared precursor of earthquake. Earthquake 1998;18(1):83–8.

[12] Gorny VI, Salman AG, Tronin AA, et al. The Earth outgoing IR radiation as an indicator of seismic activity. Proc. Acad. Sci. USSR 1988;30(1):67–9.

[13] Qiang ZJ, Xu XD, Dian CG. Thermal infrared anomaly precursor of impeding earthquakes. Chin Sci Bull 1991;36(4):319–23.

[14] Wu LX, Wang JZ. Infrared radiation features of coal and rocks under loading. Int J Rock Mech Min Sci 1998;35(7):969–76.

[15] Wu LX, Cui CY, Geng NG, Wang JZ. Remote sensing rock mechanics (RSRM) and associated experimental studies. Int J Rock Mech Min Sci 2000;37(6):879–88.

[16] Wu LX, Wu HP, Li GH. Experimental explore to thermal infrared imaging for detecting the transient process of solid impact. Chin Sci Bull 2001;46(10):872–7.

[17] Wu LX, Liu SJ, Wu YH, Wu HP. Changes in IR with rock deformation. Int J Rock Mech Min Sci 2002;39(6):825–31.

[18] Wu LX, Liu SJ, Wu YH, Li YQ. Remote sensing–rock mechanics (I): laws of thermal infrared radiation from fracturing of discontinuous jointed faults and its meanings for tectonic earthquake omens. Chin J Rock Mech Eng 2004;23(1):24–30.

[19] Wu LX, Liu SJ, Wu YH, Li YQ. Remote sensing–rock mechanics (II): laws of thermal infrared radiation from viscosity-sliding of bi-sheared faults and its meanings for tectonic earthquake omens. Chin J Rock Mech Eng 2004;23(2):192–8.

[20] Wu LX, Liu SJ, Wu YH, Li YQ. Remote sensing–rock mechanics (IV): laws of thermal infrared radiation from compressively sheared fracturing of rock and its meanings for earthquake omens. Chin J Rock Mech Eng 2004;23(4):539–44.

[21] Wu LX, Wu YH, Liu SJ, Li GH, Li YQ. Infrared radiation of rock impacted at low velocity. Int J Rock Mech Min Sci 2004;41(2):321–7.

[22] Liu SJ, Wu LX, Wu HP, et al. Quantitative study on the thermal infrared radiation of dark mineral rock in condition of uniaxial loading. Chin J Rock Mech Eng 2002;21(11):1585–9.

[23] Deng MD, Qian JD, Yin JY, et al. Research on the application of infrared remote sensing in the stability monitoring and unstability prediction of large concrete engineering. Chin J Rock Mech Eng 2001;20(2):147–50.

[24] Thomson W. Trans R Soc Edinburgh 1853;20:83–261.

[25] Nicolas A, Bouchez JL, Blaise J, et al. Geological aspects of deformation in continental shear zones. Tectonophysics 1977;42: 55–73.

[26] Fleitout L, Froidevaux C. Thermal and mechanical evolution of shear zones. J Struct Geol 1980;2:159–64.

[27] Sibson RH, et al. Power dissipation and stress levels on faults in the upper crust. J Geophys Res 1980;85:6239–47.

[28] Mounatin DS, Webber JMB. Stress pattern analysis by thermal emission (SPATE). Proc Soc Photo-Opt Inst Eng 1978;164:189.